Controllable Transmission Switch Based on Asymmetric Coupled Nonlinear Resonances

Hady Moussa,[1,2] Michele Cotrufo,[1] and Andrea Alù[1,2,3,*]

[1] *Photonics Initiative, Advanced Science Research Center, City University of New York, New York, New York 10031, USA*

[2] *Department of Electrical Engineering, City College of City University of New York, New York 10031, USA*

[3] *Physics Program, Graduate Center, City University of New York, New York, New York 10016, USA*

(Received 10 December 2022; revised 12 March 2023; accepted 21 April 2023; published 1 June 2023)

We explore the design and implementation of a passive reconfigurable switch based on nonlinear Fano resonators asymmetrically coupled to two ports. It was recently shown that asymmetric nonlinear resonators could provide passive bias-free nonreciprocal transmission when they were excited only from one port at a time. Here, we show that, by suitably exploiting time-reversal symmetry, this class of devices can also lead to controllable transmission routing, whereby a low-power pulse injected from one port controls the transmission of a larger power signal injected from the opposite port. This effect can be used to realize a power- and/or phase-controlled transmission switch with minimal power consumption. We first analyze the device with a circuit model to gain physical insights into its operation and to establish optimal operation conditions. We then provide a proof-of-principle experimental demonstration, reporting a device whereby the transmission of a 20-dBm signal can be switched from about 10% to 40% by controlling either the power or phase of a signal about 10 times weaker. This work demonstrates an alternative way to develop low-energy power-controlled reconfigurable switches for applications ranging from radar technology to wireless communications.

DOI: 10.1103/PhysRevApplied.19.064002

I. INTRODUCTION

Nonreciprocal devices, such as diodes, isolators, and circulators, are required for several applications in modern microwave, photonics, and optical systems, such as for the realization of full-duplex systems and for protecting sensitive components and sources. Since 1948, when Tellegen [1] proposed the first nonreciprocal circuit element, the *gyrator*, many research efforts have been focusing on obtaining nonreciprocal wave routing. The most adopted techniques involve using magneto-optic materials, such as ferrite-based circuits, to realize Faraday-like isolators. However, such Faraday-like isolators require the application of large magnetic fields, which result in bulky devices, and thus, they are not viable for miniaturization. Recently, a route to magnet-free nonreciprocity was proposed by using spatiotemporal modulation to implement compact circulators and isolators [2–19]. However, the applicability of these approaches is often limited by the system complexity and undesired power leakage to various harmonics. A different route to realize nonreciprocity consists of combining a nonlinear electromagnetic response, such as materials with intensity-dependent parameters, with geometrical asymmetry. Such nonlinearity-induced nonreciprocity [20,21] opens an interesting route to realize magnet-free and bias-free nonreciprocal devices [17,22–29]. A simple implementation of this nonlinearity-based nonreciprocity approach in radio-frequency (rf) circuits is sketched in Fig. 1(a). A nonlinear circuit is asymmetrically coupled to two external ports (denoted port 1 and port 2) via impedances Z_{o1} and Z_{o2}, which can be realized, for example, by quarter-wavelength transmission lines. Due to the underlying spatial asymmetry, signals with the same frequency and amplitude but injected from different ports will result in different voltages being induced inside the circuit. If one of the circuit components, for example, an internal capacitance, is nonlinear, the capacitance value will shift based on the stored voltage. This creates a situation where the circuit's resonant frequency, for a fixed input power, depends on the port from which the system is excited. By suitably tailoring the power-dependent frequency shifts, significant nonreciprocal responses can be obtained in specific power ranges [7,8,10,11], that is, the same input signal is highly transmitted when injected from port 1 [Fig. 1(b), orange rectangular pulse] or reflected when injected from port 2 [Fig. 1(c), blue rectangular pulse]. Notably, these nonreciprocal devices do not require any bias, and thus, they can

*aalu@gc.cuny.edu

be used as all-passive nonreciprocal routers. As pointed out in Ref. [30], the intrinsic nonlinear operation of these devices makes the wave-superposition principle not valid. Thus, this class of devices provides clear nonreciprocal behavior when excited only from one port at a time. For example, if the system is excited by a strong pump signal from, e.g., port 1, any weak signal *simultaneously* injected from either of the two ports is necessarily transmitted with the same efficiency [30]. This limitation follows from the fact that, under a strong excitation pump, the nonlinear dynamic equations for the transmission of weaker probes can be linearized around the pump-intensity value [21,30], and linear equations are bound to describe reciprocal propagation [31]. While a simultaneous two-port excitation is detrimental for isolation purposes, it might be exploited to unlock various functionalities of these nonlinear devices [20].

Here, we demonstrate that fundamental considerations based on time-reversal symmetry [20] can be used to design a dynamically controlled rf-transmission switch, whereby the transmission of a large signal is controlled by a much weaker controlling signal coming from the opposite port. We analyze the system theoretically and numerically to evaluate its performance in a realistic setting and to identify optimal parameter ranges. Our analysis shows that, depending on the chosen operation condition, the device can be used either as a power- or a phase-dependent dynamic transmission switch. Moreover, we provide an experimental demonstration of this concept by using printed circuit boards and lumped elements. Our experimental results show that the transmission of a 20-dBm signal can be quickly switched from about 10% to 40% by varying the power of a controlling signal, which is about 10 times weaker. Time-reversal symmetry considerations bound the minimum value of the controlling power required to trigger the switch, and by increasing the number of nonlinear coupled resonators, we may be able to reduce the controlling power to values smaller than 0.1% of the input power [20].

II. MODEL AND NUMERICAL ANALYSIS

The underlying physical mechanism to obtain a wave-controlled transmission switch is illustrated in Figs. 1(b)–1(d). As already mentioned in Sec. I, the asymmetric nonlinear circuit in Fig. 1(a) can be designed to be nonreciprocal under one-port excitation. A pulse injected from port 1 [the "forward excitation," orange pulse in Fig. 1(b)] is largely transmitted into port 2, while a small signal (blue pulse) is reflected back into port 1. Conversely, the same pulse injected from port 2 [the "backward excitation," blue pulse in Fig. 1(c)] is largely reflected. Neglecting parasitic loss and assuming that the nonlinear response is instantaneous, the circuit in Fig. 1(a) obeys time-reversal symmetry, i.e., given a valid dynamic evolution of the system in terms of ingoing and outgoing fields, the time-reversed dynamics (whereby ingoing and outgoing fields are swapped, and we perform conjugation of any complex quantity) must remain a physically valid solution. By applying this principle, we can time reverse the forward-excitation scenario, which results in the fields shown in Fig. 1(d). Now, a large pulse injected from port 2 is fully transmitted into port 1 if a weak pulse is simultaneously injected from port 1.

The switch operation is now clear by comparing Figs. 1(c) and 1(d): the port-to-port transmission of a pulse injected from port 2 is largely controlled by the input power of a much weaker pulse simultaneously injected from port 1. To rigorously implement this protocol, we would need to inject the time-reversed version of the pulses produced in the forward scenario into the system with precise synchronization compared to the incoming pulse, which may be tricky to implement, since some level of distortion and uncertainty is always present. However, as we discuss in Ref. [20], the mechanism still works well when the same pulse shape (e.g., square pulse) is used for all pulses, and the mutual phase between counterpropagating pulses is used as a knob to emulate synchronization within the band of interest and maximize the desired functionality.

To implement the working principle discussed above in rf circuits, we begin by designing, inspired by the approach in Ref. [23], a nonlinearity-based nonreciprocal circuit, as shown in Figs. 1(a) and 2(a). The circuit consists of a nonlinear resonator asymmetrically coupled to the external ports through quarter-wavelength transmission lines with unequal characteristic impedances ($Z_{o1} \neq Z_{o2}$). The resonator in the circuit [Fig. 1(a)] consists of a series LC resonator (L_s, C_s) connected in parallel with capacitance C_p. The series (L_s, C_s) is characterized by a resonant frequency and characteristic impedance of $\omega_o = 1/\sqrt{L_s C_s}$ and $Z_o = \sqrt{L_s/C_s}$, respectively. The resonance frequency, ω_o, controls the spectral position at which a transmission zero occurs, while the characteristic impedance, Z_o, quantifies the resonance bandwidth. The capacitance, C_p, is added in parallel, resonant at frequency $\omega_p = \alpha\,\omega_o$ ($\alpha > 1$), which is obtained by setting $C_p = C_s/(\alpha^2 - 1)$. We assume now that the nonlinear capacitance, C_s, is realized through a varactor [32], such that its value depends on the voltage drop, V_c, across the capacitor's terminals, following the relationship $C_s(V_c) = C_{s,0}(1 + \Delta\,|V_c|^2)$ [23], where Δ is the nonlinearity coefficient and $C_{s,0}$ is the capacitance value at very small terminal voltage. As detailed in the Appendix, the circuit analysis of the device shows that the port-to-port low-power transmission spectrum is characterized by a Fano lineshape, featuring a transmission zero and peak very close to each other. Working with devices supporting Fano lineshapes is very beneficial to enhance the nonlinear effects. Indeed, thanks to narrow and sharp linewidths of Fano resonances, very small spectral shifts (and thus, very small input powers) are required to

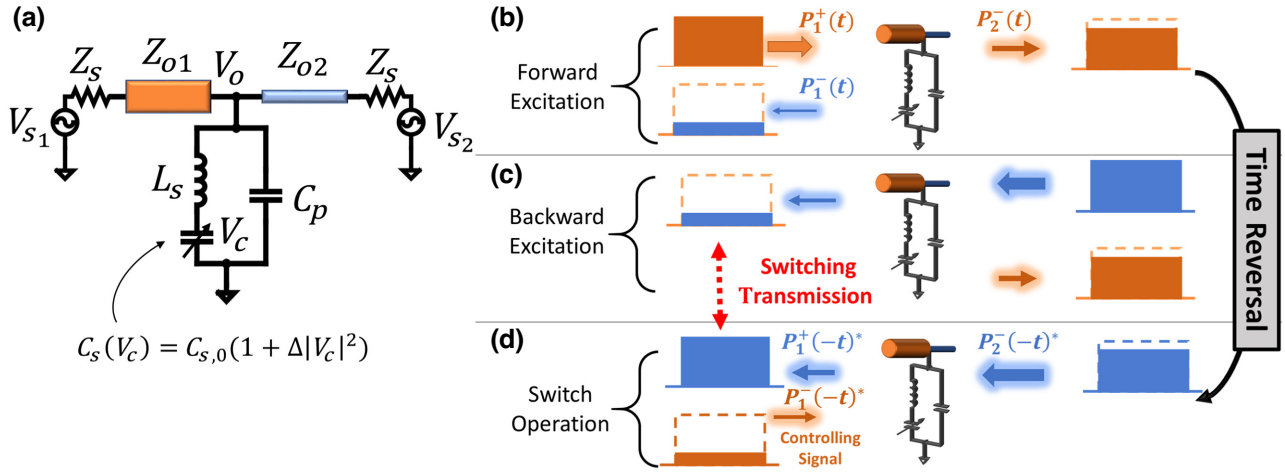

FIG. 1. (a) Schematic of the circuit considered in this work. Resonator formed by components L_s, C_s , and C_p is asymmetrically coupled to external ports through quarter-wavelength transmission lines with unequal impedances, $Z_{o1} \neq Z_{o2}$. Nonlinear capacitance $C_s(V_c)$ is implemented by two reversely connected varactors. (b)–(d) Three regimes of operation of the device, as described in the text. Blue (orange) rectangles represent ingoing (outgoing) rectangular pulses. $P_i^{\pm}$ denote ingoing (+) or outgoing (−) powers into (from) the two ports ($i = 1,2$). Blue color denotes signals flowing towards port 1, while the orange color denotes signals flowing towards port 2.

observe large transmission jumps. However, we emphasize that Fano lineshapes are not fundamentally needed to observe these effects. In its nonlinear operation, the frequencies of both transmission zero and the peak depend on the power stored in the circuit; specifically, increasing the stored power shifts the response to lower frequency. Since the coupling to the external ports is different ($Y_{o1} \neq Y_{o2}$), different voltage levels, V_c, are induced when the same power is injected from one of the two ports, resulting in different spectral shifts of the circuit response. In particular, by properly engineering the circuit parameters, at a given input power, the transmission peak when exciting from port 1 (forward excitation) can be spectrally aligned with the transmission zero when exciting from port 2 (backward excitation), leading to large nonreciprocal responses within a certain power and frequency range.

Following the guidelines outlined in more detail in the Appendix, we design a circuit for which the calculated port-to-port transmission spectra (when the system is excited from only one port) for an input power of 10 dBm are shown in Fig. 2(a). The parameters of the resonator are $L_s = 10.6$ nH, $C_s = 7.4$ pF, and $C_p = 36$ pF; the characteristic impedances are $Z_{o1} = 34.22\ \Omega$ and $Z_{o2} = 72.8\ \Omega$; and the nonlinearity coefficient is set to $\Delta = 0.1\ \mathrm{V}^{-2}$. These parameters are chosen such that in the linear regime (i.e., at low impinging powers) the transmission zero lies at a frequency of 560 MHz and the transmission peak lies at 614 MHz. As observed in Fig. 2(a), for an input power of 10 dBm both transmission zero and the peak are shifted to lower frequencies, but the magnitude of the frequency shifts depends on the excitation port. This leads to a large nonreciprocal transmission at around 544 MHz. Next, we study the case where the system is simultaneously excited from the two ports with signals of equal frequency (544 MHz) but different input amplitudes. The power of the signal injected from port 2 is fixed as $P_2^+ = 10$ dBm. According to the calculations in Fig. 2(a), such an input power would result in very low transmission from port 2 to port 1 if no other input signals were present. We then sweep the power (P_1^+) and phase ($\angle P_1^+$) of the signal injected from port 1 and record the corresponding power funneled into port 1 (P_1^-), as plotted in the color plot in Fig. 2(b). Note that in Figs. 2(b)–2(d) all input and output powers are normalized to P_2^+. For low values of impinging power P_1^+, the transmission into port 1 (P_1^-) remains low, in agreement with the single-port-excitation calculations (where $P_1^+ = 0$) in Fig. 2(a). However, as P_1^+ increases, we observe an abrupt increase in transmission, up to a value close to unity. Moreover, the phase of the control signal plays a crucial role in determining whether the transmission switch will occur and how much power, P_1^+, is required. These calculations suggest two different modes, in which the proposed device can be used as a reconfigurable or tunable transmission switch. As shown in Fig. 2(c), the power, P_1^+, at which the transmission experiences a sudden jump varies with the phase of the control signal. For example, for a phase of 94° [line denoted by B in Figs. 2(b) and 2(c)], the transmission switch occurs at a normalized power of $P_1^+/P_2^+ \approx 0.12$. For a phase of 20°, instead [line denoted by A in Figs. 2(b) and 2(c)], the threshold power is much lower, $P_1^+/P_2^+ \approx 0.02$. Besides being a low-power controllable transmission switch, the proposed device can also be used as a phase-sensitive switch. Figure 2(d) shows a one-dimensional (1D) cut from Fig. 2(b) corresponding to

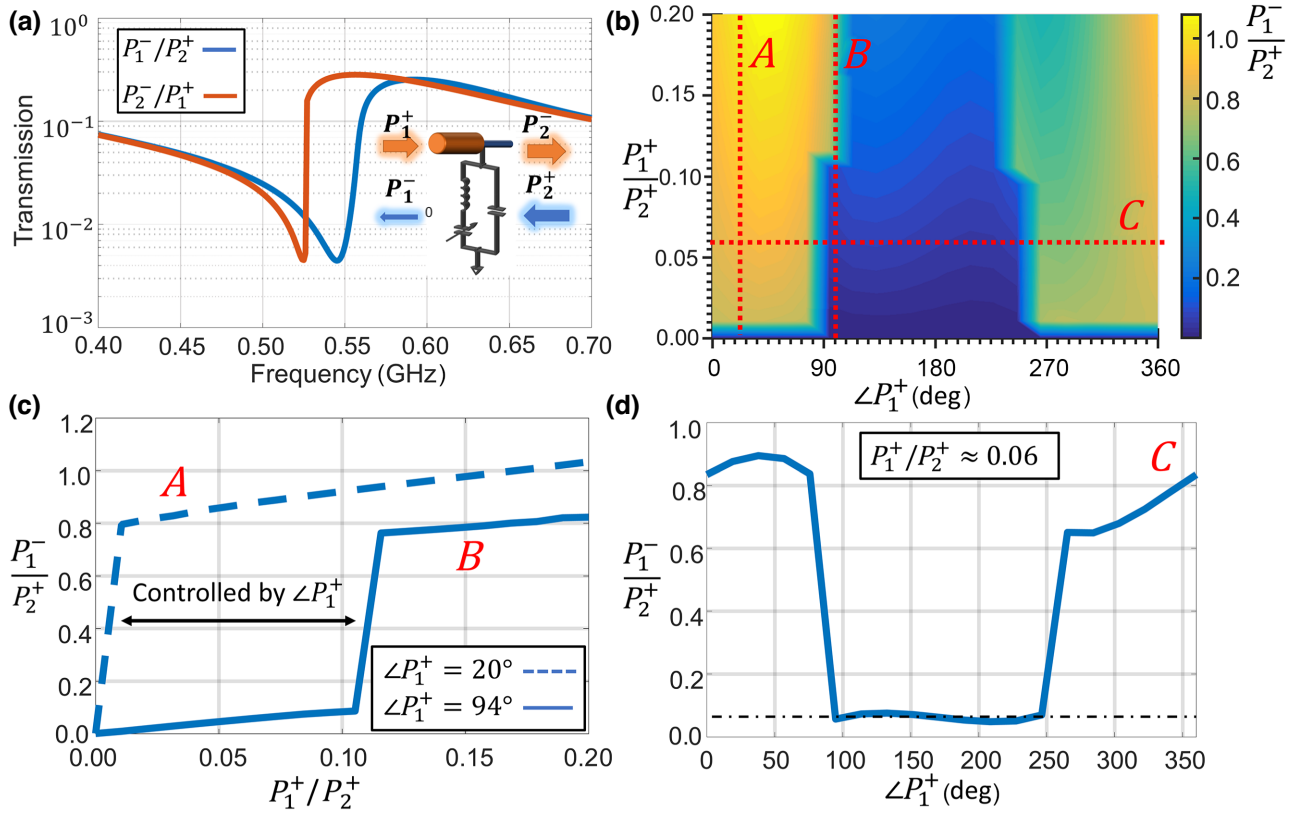

FIG. 2. (a) Calculated transmission spectrum of the proposed device when excited from only one port at a time (see text for parameter values). Device is designed such that, for the specific input power considered here, the transmission peak in the forward excitation (in orange) is aligned with the transmission zero for the backward excitation (blue). (b) Calculated power transmitted to port 1 (P_1^-) when the device is simultaneously excited from two ports versus the amplitude and phase of the power injected from port 1. Port 2 is excited with a fixed power, P_2^+. (c),(d) Cross-section 1D cuts from (b), showing the transmission into port 1 for a fixed phase of 20° and 94° [dashed and solid lines in (c)] and for fixed $(P_1^+/P_2^+) \approx 0.06$ (d).

$P_1^+/P_2^+ \sim 0.06$. Despite such a low level of power being injected from port 1, the total power transmitted into port 1 is very sensitive to the mutual phase between the two beams: in particular, the transmission into port 1 jumps from values smaller than 10% to values larger than 80% when the mutual phase between the two beams is varied by a value smaller than 10°. Thanks to its nonlinear dynamics, the device can, therefore, be used as an ultrasensitive phase sensor.

III. EXPERIMENTAL RESULTS

We fabricate and experimentally characterize the device discussed in Sec. II. As the first test, we characterize the power-dependent response of the device under test (DUT) under one-port excitation to verify the behavior predicted in Fig. 2(a). For an impinging power of 18 dBm, the device shows a large one-port nonreciprocity around the frequency of $f_o = 600$ MHz [solid lines in Fig. 3(b)]. The insertion loss and isolation are around -8 and -22 dB, respectively. The response matches the corresponding simulated results (shown in dashed lines) reasonably well.

To accurately measure the device response under two-port excitation, we build the setup shown in Figs. 3(a) and 3(b), where the input and output terminals of the DUT are cascaded with asymmetric power dividers. The power dividers allow us to inject the desired signal into each port (via a signal generator) and to simultaneously measure the outgoing signal from the same port (via a spectrum analyzer), while avoiding direct cross talk between the signal generator and the spectrum analyzer. Based on the one-port measurements in Fig. 3(b), we design the power dividers to operate at a frequency of $f_o = 600$ MHz with an unequal power-dividing ratio of 6 dB, as shown in Fig. 3(c). In the experiment, "signal generator 1" injects a fixed power of $P_{g2} \sim 20$ dBm, leading to $P_2^+ \sim |S_{12}|^2 P_{g2}$. On the other hand, "signal generator 2" generates a variable power, P_{g1}, with a tunable phase shift relative to P_{g2}, leading to power injected from port 1 being equal to $P_1^+ \sim |S_{12}|^2\, P_{g1}$. In our experiment, the output of the power divider, $P_{R,\text{meas}} = |S_{13}|^2\, P_1^- + |S_{23}|^2\, P_1^+$, is measured. Since the power divider is designed to have $S_{13} \approx -7.5$ dB and $S_{23} < -30$ dB, the contribution from the reflected term $(|S_{23}|^2\, P_1^+)$ can be neglected, and we can retrieve the

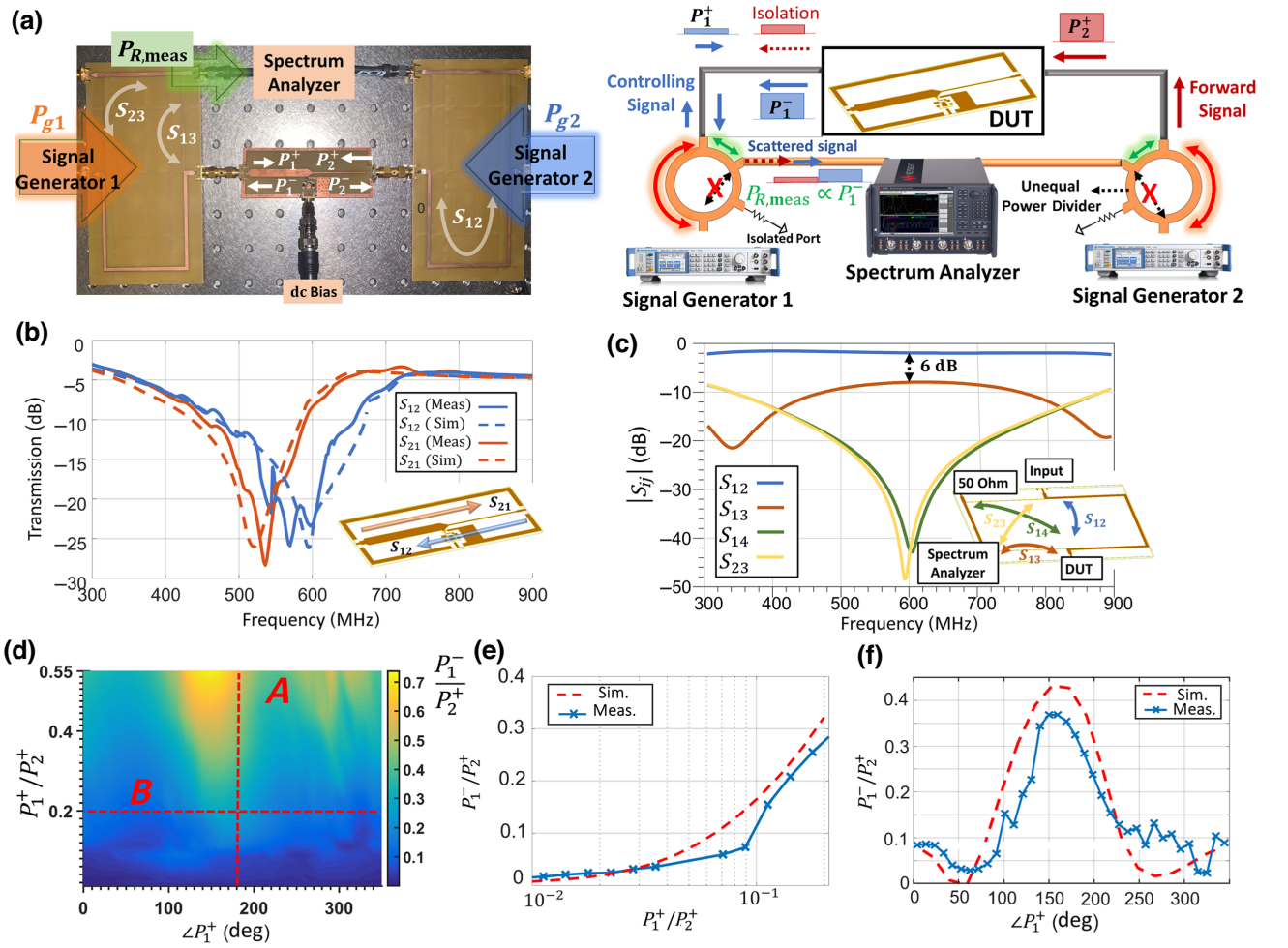

FIG. 3. (a) Photograph of the fabricated device and measurement setup. DUT in the middle is connected to unequal power dividers with 6 - dB ratio. Input of the dividers is connected to the DUT, while the divider outputs (with 30-dB isolation) are connected to the signal generators and spectrum analyzers. In the fabricated circuit, dc voltage [denoted dc bias in (a)] can be used to tune the low-power value of the varactor's capacitance. In the experiments shown here, dc bias is always set to 0. Power divider is introduced such that the spectrum-analyzer signal carries only information about the scattered signal. One of the signal generators injects a fixed high-intensity input from port 2, while the power and phase of the signal injected by the other generator is swept. (b) S parameters of the DUT when excited only from one port and for 20-dBm excitation. Operational frequency is set to 600 MHz. (c) S parameters of the fabricated power divider, together with the ports mapping to the DUT and equipment. (d) Power transmitted into port 1 for different values of magnitude and phase of the power injected into port 1. Cross-section 1D cuts corresponding to lines A (e) and B (f) from the color plot in (d), showing the transmission into port 1 for a fixed phase of 180° (e) and for fixed $(P_1^+/P_2^+) \sim 0.2$ (f). Red dashed lines correspond to simulations performed with realistic circuit parameters.

output signal, $P_1^- \approx P_{R,\mathrm{meas}}/|S_{13}|^2$. The color plot in Fig. 3(d) shows the scattered signal P_1^- for different amplitudes and phases of input power P_1^+. At low input powers, the transmission into port 1 remains small, similar to the one-port excitation scenario shown in Fig. 2(a). As the control power, P_1^+, increases, the scattered signal, P_1^-, jumps to significantly higher values for select values of the phase shift. This is shown more clearly in Fig. 3(e), which displays a vertical cross-section cut of the color plot in Fig. 3(d) for a phase shift of about 180° (solid blue line). Clear switching behavior occurs for controlling powers $P_1^+/P_2^+ < 0.1$. While the experimental measurements in Fig. 3 confirm qualitatively the behavior expected from the calculations in Fig. 2, quantitative deviations are also observed. In particular, the experimentally measured transmission switches, both versus power [Fig. 3(e)] and phase [Fig. 3(f)], are not as sharp as those in simulations. To better understand this behavior, we perform additional simulations of the device response by considering realistic values for intrinsic loss of the circuit components. The corresponding results [red dashed lines in Figs. 3(e) and 3(f)] show a closer match to the experiments. In addition, we stress that simulations are performed without cascading the DUT to the unequal power dividers. Realizing this setup

over a low-loss substrate or in a CMOS may lead to significantly improved performance metrics, such as achieving sharper transmission jumps, requiring lower controlling powers, and minimizing the footprint.

IV. CONCLUSIONS

Here, we propose and demonstrate a device to realize controllable transmission switching based on asymmetrically coupled nonlinear rf circuits supporting large nonreciprocal responses. The device is based on a simple circuit design, which ensures that the transmission of large power signals injected from one of the ports can be controlled by the amplitude and/or phase of a much weaker signal injected from the opposite port. We perform a theoretical and numerical analysis of this device to outline the operation principles and identify different regimes of operation. We also provide a proof-of-principle experimental demonstration of this concept based on a printed-circuit-board implementation, showcasing a device for which the transmission of a 20-dBm signal can be switched from about 10% to 40% by controlling either the power or phase of a signal that is about 10 times weaker. We anticipate that this performance can be highly improved by reducing parasitic loss and increasing design complexity, for instance, by adding multiple coupled resonators. In our proof-of-principle experiment, we consider scenarios where the controlling signal is constant over time. Nonetheless, the same working principle allows for dynamic modulations of the controlling signal, which would result in dynamic control of the transmission of the main signal. Overall, our work demonstrates a way to develop power-controlled reconfigurable switches, which may be extended to higher frequencies to benefit nanophotonic technologies and applications.

ACKNOWLEDGMENTS

This work is supported by the CHARM program, the Air Force Office of Scientific Research, and the Simons Foundation.

APPENDIX: CIRCUIT DESIGN FOR ONE-PORT EXCITATION

Considering the circuit in Fig. 1(a), and applying Kirchhoff's current law at node V_o, we obtain

$$\frac{Y_{o1}}{Y_o}V_{s1}+\frac{Y_{o2}}{Y_o}V_{s2}=\left[\frac{1}{Z(\omega,V_c)}-\frac{\omega}{\omega_o(\alpha^2-1)}+i\Gamma\right]V_o, \tag{A1}$$

$$V_c=-V_o\frac{1}{(\omega^2/\omega_o^2)(1+\Delta|V_c|^2)-1}, \tag{A2}$$

where $Z(\omega,V_c)=(\omega/\omega_o)-(\omega_o/\omega\ (1+\Delta|V_c|^2))$ and $\Gamma=(1/Y_sY_o)[Y_{o1}^2+Y_{o2}^2]$. Equation (A1) describes the input-output relationship, where the input signals at the two ports are given by $V_{s1,2}$ and the output signals are given by $V_{1,2}^-=V_o-(1/2)\ V_{s1,2}$. The output signals are always proportional to V_o and have a Fano-resonance profile, as shown in Fig. 2(a), i.e., there is a transmission peak and zero very close to each other. The transmission zero occurs when $Z(\omega,V_c)=0$, at frequency $\omega_Z=\omega_o/\sqrt{1+\Delta|V_c|^2}$. On the other hand, the transmission peak occurs when $(1/Z(\omega,V_c))-(\omega/\omega_o(\alpha^2-1))=0$, at frequency $\omega_p=\omega_o\sqrt{\alpha^2-1+1/(1+\Delta|V_c|^2)}$, where V_c is the voltage amplitude across the varactor terminals; it is given by Eq. (A2). The transmission zero and peak frequencies depend on voltage V_c, i.e., the power stored in the circuit, as it is determined by V_o. Increasing the power in the circuit (i.e., increasing V_c) shifts both ω_z and ω_p, thus shifting the whole response to lower frequencies. Moreover, for fixed circuit parameters, the product $\Delta\times V_c$ depends nonlinearly on the total input power into the circuit, which is, in turn, proportional to $(Y_{o1}/Y_o)V_{s1}+(Y_{o2}/Y_o)V_{s2}$. For asymmetric coupling ($Y_{o1}\neq Y_{o2}$), the same input voltage injected from different ports leads to different frequency shifts, thus potentially inducing a nonreciprocal response. To achieve maximum nonreciprocity, the nonlinear shift should be such that the transmission zero when exciting the system from one direction (named *forward excitation*) is spectrally aligned with the transmission peak obtained when exciting from the opposite direction (named *backward excitation*). This condition is obtained when

$$\sqrt{\left(1+\Delta\left|V_c^{(\mathrm{BW})}\right|^2\right)(\alpha^2-1)+\frac{1+\Delta\left|V_c^{(\mathrm{BW})}\right|^2}{1+\Delta\left|V_c^{(\mathrm{FW})}\right|^2}}=1, \tag{A3}$$

where $V_c^{(x)}$ is the voltage across the varactor's terminals upon forward ($x=$"FW") and backward ($x=$"BW") excitation. For fixed values of circuit parameters, Eq. (A3) is a function of the operation frequency, ω, and the input voltage, $V_{s1,2}$. Consequently, to maximize the nonreciprocal response, Eqs. (A1) and (A2) are solved for different input powers and operation frequency, and Eq. (A3) is used to find the optimal operation point.

As mentioned in Sec. I, the nonlinear device in Fig. 1(a) cannot work as a true isolator when the two ports are simultaneously excited, due to dynamic reciprocity [30]. This can be further explained with Eq. (A1) as follows: in the forward-excitation scenario, $V_{s2}=0$, and in Eq. (A1), the input voltage is $(Y_{o1}/Y_o)V_{s1}$, which results in a frequency shift proportional to $\Delta|V_c^{(\mathrm{FW})}|^2$. On the other hand, for backward excitation, the input voltage in Eq. (A1) is $(Y_{o2}/Y_o)V_{s2}$, which results in a frequency shift

proportional to $\Delta|V_c^{(\mathrm{BW})}|^2$. This results in a transmission zero at the frequency of operation for backward excitation. In the case of simultaneous two-port excitation, the input voltage is $(Y_{o1}/Y_o)V_{s1} + (Y_{o2}/Y_o)V_{s2}$. Thus, the frequency shift depends on a coherent superposition of the two input powers, thus allowing the coherent control of the port-to-port transmission discussed in the main text.

[1] B. D. Tellegen, The gyrator, a new electric network element, Philips Res. Rep. **3**, 81 (1948).

[2] A. Kord, D. L. Sounas, and A. Alu, Microwave nonreciprocity, Proc. IEEE **108**, 1728 (2020).

[3] D. L. Sounas and A. Alù, Nonreciprocal photonics based on time modulation, Nat. Photonics **11**, 774 (2017).

[4] R. Lu, T. Manzaneque, Y. Yang, A. Gao, L. Gao, and S. Gong, in *2018 IEEE International Ultrasonics Symposium (IUS)* (IEEE, 2018), pp. 1–4.

[5] A. Nagulu, N. Reiskarimian, and H. Krishnaswamy, Nonreciprocal electronics based on temporal modulation, Nat. Electron. **3**, 241 (2020).

[6] D. Karki, V. Stenger, A. Pollick, and M. Levy, Broadband bias-magnet-free on-chip optical isolators with integrated thin film polarizers, J. Lightwave Technol. **38**, 827 (2020).

[7] A. Mekawy, D. L. Sounas, and A. Alù, Free-space nonreciprocal transmission based on nonlinear coupled Fano metasurfaces, Photonics **8**, 139 (2021). MDPI.

[8] P. Yang, X. Xia, H. He, S. Li, X. Han, P. Zhang, G. Li, P. Zhang, J. Xu, Y. Yang, T. Zhang, Realization of Nonlinear Optical Nonreciprocity on a Few-Photon Level Based on Atoms Strongly Coupled to an Asymmetric Cavity, Phys. Rev. Lett. **123**, 233604 (2019).

[9] K. Van Gasse, M. Cotrufo, K. Yang, A. Alù, and J. Vuckovic, in *CLEO: Science and Innovations* (Optica Publishing Group, 2022), pp. SM4O. 2.

[10] D. M. Solís and N. Engheta, Nonreciprocal Epsilon-Near-Zero-Dielectric Bilayers: Enhancement of Nonreciprocity from a Nonlinear Transparent Conducting Oxide Thin Film at Epsilon-Near-Zero Frequency, Phys. Rev. Appl. **17**, 034053 (2022).

[11] M. Moccia, G. Castaldi, V. Galdi, A. Alu, and N. Engheta, Optical isolation via unidirectional resonant photon tunneling, J. Appl. Phys. **115**, 043107 (2014).

[12] Y. Hu, Yihong Qi, Yu You, Shicheng Zhang, Gongwei Lin, Xiaolin Li, Jiangbin Gong, Shangqing Gong, and Yueping Niu, Passive Nonlinear Optical Isolators Bypassing Dynamic Reciprocity, Phys. Rev. Appl. **16**, 014046 (2021).

[13] B. Jin and C. Argyropoulos, Self-Induced Passive Nonreciprocal Transmission by Nonlinear Bifacial Dielectric Metasurfaces, Phys. Rev. Appl. **13**, 054056 (2020).

[14] S. V. Zhukovsky and A. G. Smirnov, All-optical diode action in asymmetric nonlinear photonic multilayers with perfect transmission resonances, Phys. Rev. A **83**, 023818 (2011).

[15] L. Ren, X. Xu, S. Zhu, L. Shi, and X. Zhang, Experimental realization of on-chip nonreciprocal transmission by using the mechanical Kerr effect, ACS Photonics **7**, 2995 (2020).

[16] L. Del Bino, J. M. Silver, X. Zhao, S. L. Stebbings, and P. Del'Haye, in *2017 Conference on Lasers and Electro-Optics (CLEO)* (IEEE, 2017), pp. 1–2.

[17] L. Del Bino, J. M. Silver, M. T. Woodley, S. L. Stebbings, X. Zhao, and P. Del'Haye, Microresonator isolators and circulators based on the intrinsic nonreciprocity of the Kerr effect, Optica **5**, 279 (2018).

[18] L. Fan, L. T. Varghese, J. Wang, Y. Xuan, A. M. Weiner, and M. Qi, Silicon optical diode with 40 dB nonreciprocal transmission, Opt. Lett. **38**, 1259 (2013).

[19] P. K. Sahoo and J. Joseph, Optical diode using nonlinear polystyrene ring resonators in two-dimensional photonic crystal structure, Appl. Opt. **52**, 8252 (2013).

[20] M. Cotrufo, S. A. Mann, H. Moussa, and A. Alù, Nonlinearity-induced nonreciprocity–part II, IEEE Trans. Microwave Theory Tech. **69**, 3584 (2021).

[21] M. Cotrufo, S. A. Mann, H. Moussa, and A. Alù, Nonlinearity-induced nonreciprocity–part I, IEEE Trans. Microwave Theory Tech. **69**, 3569 (2021).

[22] G. D'Aguanno, D. L. Sounas, H. M. Saied, and A. Alù, Nonlinearity-based circulator, Appl. Phys. Lett. **114**, 181102 (2019).

[23] D. L. Sounas, J. Soric, and A. Alu, Broadband passive isolators based on coupled nonlinear resonances, Nat. Electron **1**, 113 (2018).

[24] D. Sounas, J. Soric, G. D'Aguanno, and A. Alù, in *2018 12th International Congress on Artificial Materials for Novel Wave Phenomena (Metamaterials)* (IEEE), pp. 364–366.

[25] A. R. Hamann, Clemens Müller, Markus Jerger, Maximilian Zanner, Joshua Combes, Mikhail Pletyukhov, Martin Weides, Thomas M Stace, Arkady Fedorov, Nonreciprocity Realized with Quantum Nonlinearity, Phys. Rev. Lett. **121**, 123601 (2018).

[26] D. L. Sounas and A. Alù, Fundamental bounds on the operation of Fano nonlinear isolators, Phys. Rev. B **97**, 115431 (2018).

[27] L. Del Bino, J. M. Silver, S. L. Stebbings, and P. Del'Haye, Symmetry breaking of counterpropagating light in a nonlinear resonator, Sci. Rep. **7**, 1 (2017).

[28] K. Xia, F. Nori, and M. Xiao, Cavity-Free Optical Isolators and Circulators Using a Chiral Cross-Kerr Nonlinearity, Phys. Rev. Lett. **121**, 203602 (2018).

[29] B. Jin and C. Argyropoulos, Nonreciprocal transmission in nonlinear *PT*-symmetric metamaterials using epsilon-near-zero media doped with defects, Adv. Opt. Mater. **7**, 1901083 (2019).

[30] Y. Shi, Z. Yu, and S. Fan, Limitations of nonlinear optical isolators due to dynamic reciprocity, Nat. Photonics **9**, 388 (2015).

[31] A. B. Khanikaev and A. Alù, Nonlinear dynamic reciprocity, Nat. Photonics **9**, 359 (2015).

[32] A. S. Sedra, K. C. Smith, T. C. Carusone, and V. Gaudet, *Microelectronic circuits* (Oxford university press, New York, 2004).